14
Detector systems

Particle physics experiments are conceived to study some aspect of particle properties or of the interactions between particles. The first step in designing an experiment is to find an efficient trigger for the desired experiment. Then one must select suitable detectors to gather the necessary data. Often the choice of detectors and their configuration involves compromises between competing goals. In this chapter we will examine some important considerations involved in designing a detector system.

14.1 Magnetic spectrometers

A spectrometer, as the word is generally used, is a system for measuring the momentum of a particle. The spectrometer consists of a magnet and tracking detectors that determine the momentum through a measurement of the particle's curvature. The motion of a particle with charge q in a magnetic field B is governed by the equation

$$d\mathbf{p}/dt = q/c\ \mathbf{v} \times \mathbf{B} \tag{14.1}$$

If the field is uniform and we neglect the presence of matter in the particle's path, the magnitude of the momentum remains constant with time and the particle will follow a helical trajectory. The actual trajectory will differ from an exact helix due to spatial inhomogeneities in the magnetic field and radiation energy losses. If matter is present, there will be additional changes in the trajectory due to ionization energy loss and multiple scattering.

The momentum is related to B and the radius of curvature ρ by

$$p = 0.2998B\rho \qquad \text{GeV}/c,\ \text{T},\ \text{m} \tag{14.2}$$

The radius of curvature, chord l, and sagitta s of the circular segment shown in Fig. 14.1 are related by

Downloaded from https://www.cambridge.org/core. UNIVERSIDAD AUTONOMA METROPOLITANA, on 15 Nov 2026 at 14:08:38, subject to the Cambridge Core terms of use, available at https://www.cambridge.org/core/terms. https://doi.org/10.1017/9781009290098.015

$$\rho = \frac{l^2}{8s} + \frac{s}{2}$$
$$\simeq \frac{l^2}{8s} \tag{14.3}$$

The accuracy in the determination of p is related by Eq. 14.2 to the accuracy in the measurement of ρ. This is in turn related by Eq. 14.3 to the accuracy in determining the sagitta of the arc. Thus we have

$$p = 0.3\,\frac{Bl^2}{8s} \tag{14.4}$$

$$\left|\frac{\delta p}{p}\right| = \left|\frac{\delta s}{s}\right| \tag{14.5}$$

The quantity $\delta p/p$ is referred to as the momentum resolution. We see that the momentum resolution is equal to the relative error in the sagitta determination. In addition to the deviations of the trajectory from a perfect helix mentioned earlier, the resolution of the tracking detectors (setting error) and distortions in the measuring system contribute to δs.

Gluckstern [1] has shown that the error in the curvature ($k = 1/\rho$) due to measurement error is

$$\delta k = (\epsilon/L^2)\sqrt{A_N} \tag{14.6}$$

where ϵ is the rms measurement error, L is the projected track length in the magnetic field, and A_N is a parameter that depends on the number N of points that are measured. For large N

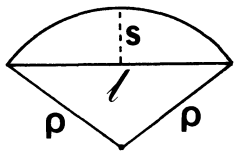
$$A_N = \frac{720}{N+5} \tag{14.7}$$

The contribution to the momentum resolution from measurement error then is

$$\left|\frac{\delta p}{p}\right| = \sqrt{A_N}\,\frac{\epsilon}{L^2}\,\frac{p}{0.3B} \tag{14.8}$$

We see that the resolution is improved faster by increasing L than by increasing B or decreasing ϵ.

Figure 14.1 The sagitta (s), chord (l), and radius (ρ) of a circular arc.



Downloaded from https://www.cambridge.org/core. UNIVERSIDAD AUTONOMA METROPOLITANA, on 15 Nov 2026 at 14:08:38, subject to the Cambridge Core terms of use, available at https://www.cambridge.org/core/terms. https://doi.org/10.1017/9781009290098.015

The error in the curvature due to multiple scattering is

$$\delta k_{\text{ms}} = \sqrt{\xi C_N / L} \tag{14.9}$$

where ξ is the rms projected angle per unit thickness due to multiple scattering and C_N is a parameter that equals 1.43 for large N. The contribution to the momentum resolution is

$$\left|\frac{\delta p}{p}\right| = \frac{p}{0.3B}\sqrt{\frac{\xi C_N}{L}} \tag{14.10}$$

The trajectory of a particle before and after the magnet can be determined using wire chambers or scintillator telescopes. Assume we have a uniform magnetic field that ends abruptly near the magnet edges. The entrance and exit angles are related to the bending in the field by the relation

$$\sin\beta_{\text{i}} + \sin\beta_{\text{o}} = \frac{\int B\,dl}{3.33p} \qquad \text{GeV}/c,\ \text{T},\ \text{m} \tag{14.11}$$

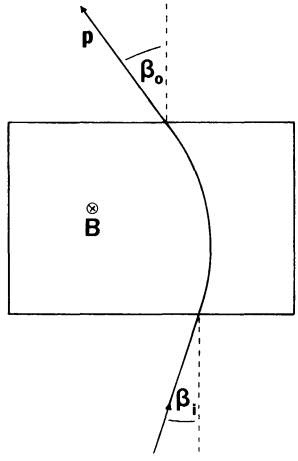
as shown in Fig. 14.2. This equation can be used to determine p once the magnetic field has been accurately measured. The momentum resolution is related to the error in determining the total bend angle by

$$\frac{\delta p}{p} \simeq \frac{\delta\alpha}{\alpha} \simeq \frac{3.33\,\Delta x\, p}{r\int B\,dl} \tag{14.12}$$

where r is the distance to the counter, and

$$\delta\alpha = \Delta x / r \tag{14.13}$$

Figure 14.2 Geometry of a particle orbit through a bending magnet.



Downloaded from https://www.cambridge.org/core. UNIVERSIDAD AUTONOMA METROPOLITANA, on 15 Nov 2026 at 14:08:38, subject to the Cambridge Core terms of use, available at https://www.cambridge.org/core/terms. https://doi.org/10.1017/9781009290098.015

A number of methods have been used to map out the magnetic field in spectrometer magnets. The field may be quite nonuniform since the magnets tend to have large gaps to maximize the solid angle available to the experiment. Common methods for measuring the field include rotating coils, nuclear magnetic resonance, or Hall probes. Usually the three components of the field are measured for many points over a large mesh. The data is sometimes fit to a high-order polynomial for calculational convenience. Amako et al. [2] have described an automated Hall probe system used for field mapping at KEK. The temperature-compensated Hall probes were mounted in a copper block and positioned on a movable table using computer-controlled stepping motors. Different field components were measured by rotating the probe orientation. The uncertainty in the field was less than 32 G everywhere in the magnet volume for a 12.8-kG central field.

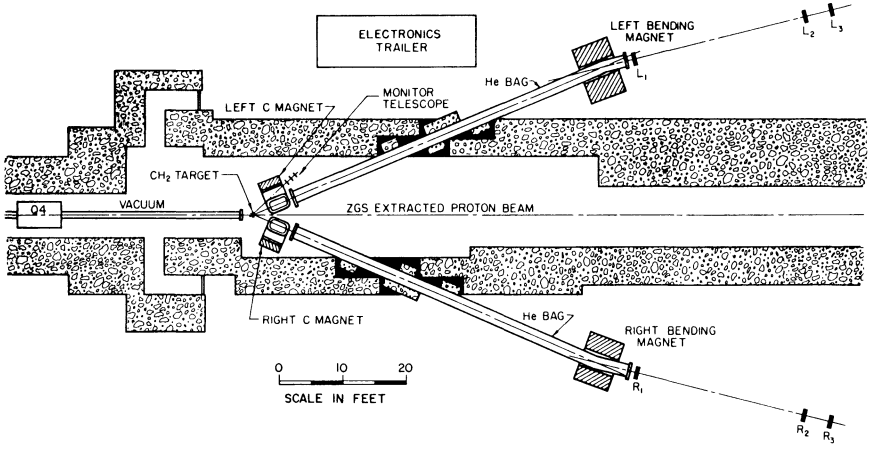
Now consider as an example the double arm spectrometer shown in Fig. 14.3. The spectrometer was used in an experiment to study pp elastic scattering at 90° in the center of mass between 5 and 13 GeV/c [3]. Each arm consisted of two bending magnets and a three-counter scintillator telescope to measure the exit angle. For 90° CM scattering both final state protons emerge at the same angle in the laboratory.

The solid angle acceptance of this type of spectrometer is given by

$$\Delta\Omega = A/r^2 \tag{14.14}$$

where A is the area of the defining counter in the telescope and r is its distance from the target. For the 7×5-in.^{2} counter located about 100 ft

Figure 14.3 A simple two-arm spectrometer. The beam enters from the left. (C. Akerlof et al., Phys. Rev. 159: 1138, 1967.)



Downloaded from https://www.cambridge.org/core. UNIVERSIDAD AUTONOMA METROPOLITANA, on 15 Nov 2026 at 14:08:38, subject to the Cambridge Core terms of use, available at https://www.cambridge.org/core/terms. https://doi.org/10.1017/9781009290098.015

from the target this corresponds to a solid angle of 24 μsr. There is a correction to the actual acceptance due to focusing at the edges of the dipole magnets.

In principle, the R counter should be identical to the L counter. However, in this case the finite target size, beam divergence, multiple scattering, and field integral error could lead to a loss of true coincidences by allowing the companion of a proton detected in the L arm to escape from the R arm. For this reason, the R counter was slightly larger than the corresponding L counter. The C magnets were used to ensure that the protons always entered the bending magnets at the same angle and approximately the same location. This permitted the study of elastic scattering at a large number of incident momenta without moving the bending magnets or counter telescopes.

The momentum resolution is related to the spatial and angular divergences of the beam by

$$\Delta x = \alpha_1 \, \Delta\theta_0 + \alpha_2 \, \Delta p_0/p_0 \tag{14.15}$$

The quantity $\Delta\theta_0$ can be related to $\Delta p_0/p_0$ by the kinematics of elastic scattering. The α_i are beam transport matrices. Thus, the momentum resolution will be determined by the counter width Δx.

The normalized number of left–right coincidences is shown in Fig. 14.4 as a function of the current in the right bending magnet. The number of events peak at the calculated value for elastic scattering. The plateau around the elastic point is due to the overmatching of the R counters. As the current deviates from the value for elastic scattering, the event rate decreases rapidly.

14.2 Design considerations

The design of a detector system is ultimately determined by the physics goals that are being pursued [4]. There is no universal spectrometer capable of measuring all high energy processes. Each system must emphasize certain features important to the physical processes under study to the detriment of others. "Known" physics questions can be addressed using smaller, specialized detectors, but searches for "new" physics require a general purpose detector system.

The first obvious consideration is whether the experiment will be performed at a fixed target or colliding beam accelerator. Fixed target spectrometers can benefit from the Lorentz transformation, which folds the full CM angular range into the forward direction in the LAB. These spectrometers tend to be long and of small transverse extent. Colliding beam spectrometers, on the other hand, derive no such solid angle benefit

Downloaded from https://www.cambridge.org/core. UNIVERSIDAD AUTONOMA METROPOLITANA, on 15 Nov 2026 at 14:08:38, subject to the Cambridge Core terms of use, available at https://www.cambridge.org/core/terms. https://doi.org/10.1017/9781009290098.015

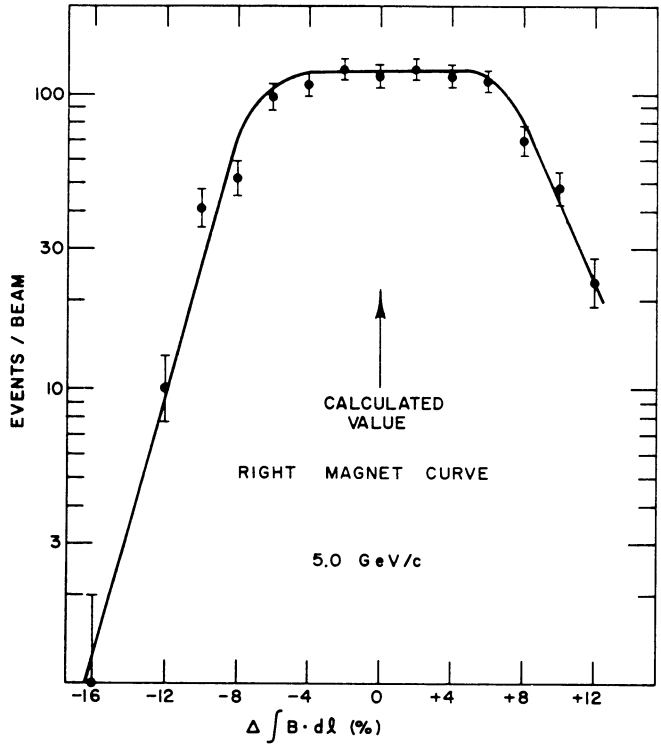
and must completely surround the interaction region to obtain full CM coverage.

A second consideration is the nature of the beam particles. In e^+e^- colliding beams with customary luminosities, the event rates are small and every event can be recorded. In proton machines the fact that the particles interact strongly and that the luminosities tend to be higher results in much higher event rates. Here an efficient trigger system is essential to reduce the data rate to manageable levels.

Electrons in linear accelerators are accelerated in very short pulses with a very high repetition rate. This beam structure makes it very difficult to use time coincidence techniques to identify events [5]. Electron interactions are also associated with intense electromagnetic showers in the forward direction, and the detector design must allow for this.

There are five major areas of concern in most detector systems: magnetic field, tracking chambers, calorimetry, particle identification, and

Figure 14.4 Left–right coincidences in the spectrometer of Fig. 14.3 as a function of the current in the right bending magnet. (C. Akerlof et al., Phys. Rev. 159: 1138, 1967.)



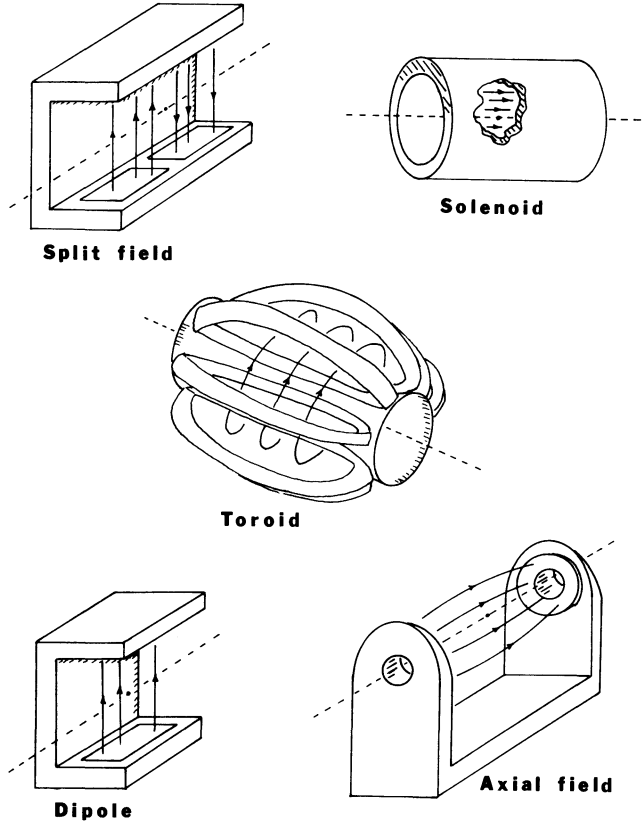
Downloaded from https://www.cambridge.org/core. UNIVERSIDAD AUTONOMA METROPOLITANA, on 15 Nov 2026 at 14:08:38, subject to the Cambridge Core terms of use, available at https://www.cambridge.org/core/terms. https://doi.org/10.1017/9781009290098.015

triggering. The physics goals will determine the relative importance of each. Most spectrometers employ a magnetic field and tracking chambers to measure the charge and momentum of any charged particles. However, there are detector systems, such as the Crystal Ball described in Section 14.4, that do not use a magnetic field.

The choice of magnetic field configuration puts severe constraints on the design of the spectrometer [6, 7]. Figure 14.5 depicts five magnetic field configurations for use with colliding beams, while Table 14.1 compares some of their characteristics. The magnetic field and the tracking chambers are chosen to obtain good momentum resolution for tracks in the region of most importance. The field cannot be too high or else large numbers of small momentum tracks will spiral through the chambers.

Dipole magnets typically have the field perpendicular to the incident beam. They are used with proton beams, but usually not in e^+e^- machines

Figure 14.5 Magnetic field configurations used with colliding beams.



Downloaded from https://www.cambridge.org/core. UNIVERSIDAD AUTONOMA METROPOLITANA, on 15 Nov 2026 at 14:08:38, subject to the Cambridge Core terms of use, available at https://www.cambridge.org/core/terms. https://doi.org/10.1017/9781009290098.015

because of synchrotron radiation. Dipoles are good for analyzing forwardly produced particles, which makes them well suited for fixed target accelerators. In addition, they are quite flexible for changing external devices. For colliding beam machines the deflection of the beams must be compensated for by another magnet. This can be avoided in a split field magnet, in which the direction of the field reverses in the magnet center.

Since the field in solenoid magnets is approximately parallel to the beam direction, only a weak compensating magnet may be required. The combination of a solenoid magnet and cylindrical tracking chambers has been widely adopted at e^+e^- colliding beam machines. Solenoids provide uniform azimuthal acceptance and do not disturb the transverse momenta of particles. However, only a limited transverse space is available before entering the coils. A solenoidal field with open access around polar angles of 90° is provided by an axial field magnet (AFM). A spectrometer built around this type of magnet is described in Section 14.4.

Lastly, we mention the toroidal field configuration. Here a large p_t particle must cross the coils and magnet structural elements before entering the magnetic field. The field itself is nonuniform, varying as

$$B(r) = \frac{B_i r_i}{r} \tag{14.16}$$

where B_i is the field at the inner radius r_i. The design is most useful in a muon spectrometer. In this case the fact that the coils are in the particle path is no problem, since the detector invariably has a massive hadronic filter. Multiple scattering limits the ultimate momentum resolution. One interesting feature of the toroid is that the field lines form circles around

Table 14.1. *Comparison of magnetic field configurations*

	Dipole	Split field magnet	Solenoid	Axial field magnet	Toroid
Return yoke	yes	yes	yes	yes	no
Compensating magnet	yes	no	small	small	no
e^+e^- beams	no	no	yes	yes	yes
Coils before field region	no	no	no	no	yes
High p_t measurement	good	good	poor	good	poor
Forward particle measurement	good	good	poor	poor	poor

Source: W. Willis, Phys. Today, Oct. 1978, p. 32; T. Taylor, Physica Scripta 23: 459, 1981.

Downloaded from https://www.cambridge.org/core. UNIVERSIDAD AUTONOMA METROPOLITANA, on 15 Nov 2026 at 14:08:38, subject to the Cambridge Core terms of use, available at https://www.cambridge.org/core/terms. https://doi.org/10.1017/9781009290098.015

the beam and no iron return yoke is necessary. The field can be reversed to check systematic effects without affecting the beam.

Particle tracking in colliding beam detectors is usually done in a central detector that surrounds the intersection point. It is the job of the central detector to measure the momenta, directions, and multiplicity of charged tracks coming from the interaction. The central detector usually consists of drift chambers or MWPCs but may include a high resolution vertex detector or a TPC.

Some important "typical" characteristics of MWPCs, drift chambers, and other detectors used for tracking are given in Table 14.2. The desired momentum resolution, ability to distinguish tracks in high multiplicity events, and expected rates determine the solid angle coverage, wire spacing, and rate capabilities of the chambers.

Calorimeters may be desirable to measure the influence of neutral particles and the production of electrons and photons. We have discussed the characteristics of sampling calorimeters in Chapter 11. Table 14.3 contains a summary of some important properties of "continuous" calorimeters. The best resolution has been obtained with NaI crystals, whose resolution typically improves with energy according to the relation, $\sigma_E/E \sim 2\%/E^{1/4}$ with E in GeV. BaF_2 is a promising material for calorimeter applications [8]. It scintillates in the ultraviolet portion of the spectrum with a decay time of only 0.6 ns. It is nonhygroscopic and cheaper than BGO. A calorimeter may be used in the trigger to achieve large event rate reductions in proton machines.

Some experiments look for the production of specific types of particles.

Table 14.2. *Typical properties of tracking detectors*

	Spatial resolution (μm)	Response time (ns)	Recovery time (ns)
Scintillator hodoscope	5000	10	10
MWPC	500	100	[a]
Drift chamber	150	100–1000	[a]
Proportional drift tubes	5000	400	100
Bubble chamber	100	10^6	10^7
Spark chamber	300	1000	10^6
Streamer chamber	200	1000	10^6
Flashtube hodoscope	5000	1000	10^6

[a] Individual wire dead for ~100 ns. Other wires are still sensitive.

Downloaded from https://www.cambridge.org/core. UNIVERSIDAD AUTONOMA METROPOLITANA, on 15 Nov 2026 at 14:08:38, subject to the Cambridge Core terms of use, available at https://www.cambridge.org/core/terms. https://doi.org/10.1017/9781009290098.015

Downloaded from https://www.cambridge.org/core. UNIVERSIDAD AUTONOMA METROPOLITANA, on 15 Nov 2026 at 14:08:38, subject to the Cambridge Core terms of use, available at https://www.cambridge.org/core/terms. https://doi.org/10.1017/9781009290098.015

Table 14.3. *Continuous calorimeters*

	Statistical contribution to energy resolution $cE^{-1/2}$ c[%]	Typical integration time [ns]	Radiation length (cm)	Absorption length (cm)	Relative light output	Radiation for 10% loss (rad)
Lead glass (SF5)	4.5	40	2.5	42	1	2500
Scintillation glass (SCG1-C)	1.1	100	4.35	45	5.1	8.5×10^4
BGO	1	300	1.12	23	10^3	10^4–10^5
NaI	1[a]	250	2.5	41	10^4	10^5
BaF_2	1.7	—	2.1	—	700	—

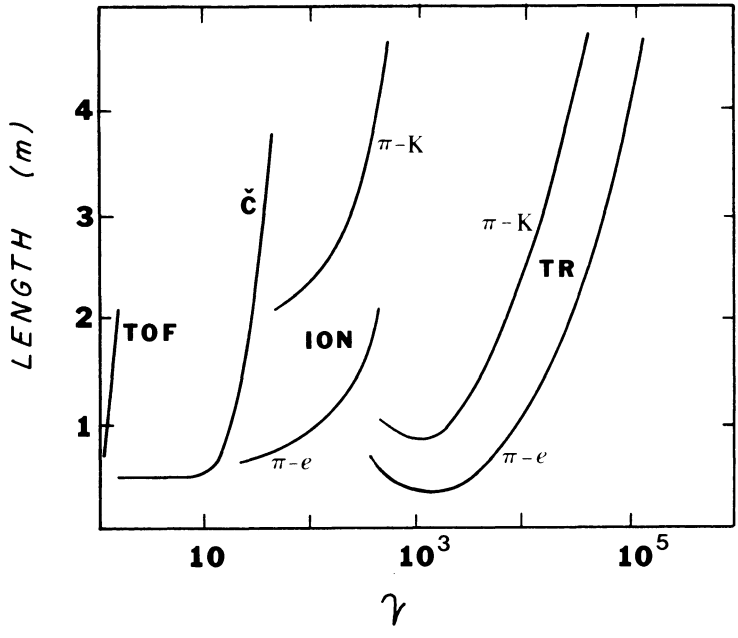
[a] Energy resolution $\sim 1\%\ E^{-1/4}$.

Source: B. Pope, Calorimetry: working group summary report, in Proc. of the 1983 DPF workshop on collider detectors, LBL-15973, UC-37, CONF-830224, p. 49.

In this case some type of particle identification must be incorporated into the design. We have discussed a number of techniques for accomplishing this in the preceding chapters. The detector space available for this purpose may be limited, particularly in colliding beam machines.

For most identification methods the accuracy of the measurement improves with length. Thus we can make a useful comparison of techniques by plotting the length required to achieve a given accuracy as a function of the energy [6]. Figure 14.6 shows that the required length grows very rapidly. At low energies time of flight and Cerenkov counter systems can be used. For large γ the intensity from transition radiation is sufficient for e/π/K separation and synchrotron radiation may be used for electron identification. There is no "natural" system for the intermediate region. One typically uses the relativistic rise of the ionization energy loss. However, because of the non-Gaussian statistical nature of the energy loss, a very large number of samples must be taken. In general, we note that π/K separation is more difficult than π/e.

Figure 14.6 The length necessary for particle identification using various techniques is shown as a function of the Lorentz factor γ. (TOF) time of flight, (C) Cerenkov counters, (ION) relativistic rise of ionization energy loss, and (TR) transition radiation. (After W. Willis, Phys. Today, Oct. 1978, p. 32.)



Downloaded from https://www.cambridge.org/core. UNIVERSIDAD AUTONOMA METROPOLITANA, on 15 Nov 2026 at 14:08:38, subject to the Cambridge Core terms of use, available at https://www.cambridge.org/core/terms. https://doi.org/10.1017/9781009290098.015

Lastly, some means of triggering must be provided and integrated into the detector system. Scintillation counters, Cerenkov counters, MWPCs, and calorimeters are typical trigger elements. The trigger timing and rate must be carefully incorporated into the overall data acquisition system.

Special care must be taken in designing a detector for use in a high luminosity environment. The major problems are the pileup of unrelated events within the detector's resolving time, rate limitations on detector operation, and the effects of radiation damage. Specialized experiments can handle the problem by using a limited solid angle acceptance. A general detector must use finer spatial segmentation of detector elements. The analog signals must be very fast, and the readout time must be as short as possible. A calorimeter can be used to provide a selective trigger.

Summaries of the important features and diagrams of many spectrometers can be found in the literature [9]. Darriulat [10] has given a summary of high p_t spectrometers, while Fabjan and Ludlam [11] have tabulated properties of many spectrometers that use calorimeters. The characteristics of the PETRA detectors have been reviewed by Wu [12].

14.3 Fixed target spectrometers

In this section we will consider the design of several spectrometers used at fixed target accelerators. Table 14.4 lists some examples of fixed target spectrometers and summarizes some of their important characteristics. The word spectrometer is used here in the more general sense of an integrated system of detectors. The spectrometers listed in Table 14.4 divide naturally into two classes. The neutrino spectrometers emphasize calorimetry and muon detection, while the charged beam spectrometers are likely to give more weight to tracking and particle identification. It should be pointed out that many of these detectors are really facilities, so that experiment dependent equipment may be used to augment the basic spectrometer.

As an example consider the European Muon Collaboration spectrometer at CERN [13]. The spectrometer operates in a secondary muon beamline at the SPS. Its primary objective is the study of "deep" inelastic scattering. In this process the beam muon interacts in the target and produces a final state muon together with other unspecified particles. The spectrometer is designed to have a large acceptance for detecting the final state muon and to make a precise measurement of its production angle and momentum.

The layout of the spectrometer is given in Fig. 14.7. The incoming beam is defined with the beam hodoscope (BH). The spray of muons

Downloaded from https://www.cambridge.org/core. UNIVERSIDAD AUTONOMA METROPOLITANA, on 15 Nov 2026 at 14:08:38, subject to the Cambridge Core terms of use, available at https://www.cambridge.org/core/terms. https://doi.org/10.1017/9781009290098.015

traveling off the beam axis (beam halo) is eliminated by using the hodoscopes (V) as veto counters in the trigger. Liquid hydrogen, liquid deuterium, and active iron-scintillator calorimeter targets have been used. A polarized target was also used to provide spin information. The target was placed close to the magnet to provide good acceptance.

The momentum determination was made using a large aperture window frame type dipole magnet (FSM) with a bending power of 5 T-m. The entrance and exit angles are measured with drift chambers (W) before and after the magnet. The chambers have a spatial resolution of ~ 0.3 mm. Tracking inside the magnetic field is done using MWPCs (P1 – P3). These chambers have a short resolving time (75 ns) to help eliminate out of time tracks, such as knock-on electrons from the target. The momentum resolution was $\sim 1\%$ for a 100-GeV/c secondary track from liquid hydrogen.

A secondary muon emerging from an interaction will pass through H3 and H4. The muon trajectory after the absorber is measured using the drift chambers W6 and W7. The single muon trigger discussed in Chapter 13 requires a track after the absorber and the absence of a beam veto. In addition, correlations are required between hodoscope planes such that (1) the track points at the target in x and y, (2) the momentum exceeds some minimum requirement, and (3) the scattering angle exceeds a preselected value.

Pions and kaons can be identified over certain momentum ranges using the gas threshold Cerenkov counter (C2) downstream of the target. The calorimeter (H2) consists of a front section of 20 radiation lengths of lead and scintillator to detect photons and electrons and 5 interaction lengths of iron and scintillator to detect hadrons. This is followed by 10 interaction lengths of magnetized iron to absorb the remaining hadrons.

A partial view of another large fixed target detector system is shown in Fig. 14.8. The CHARM detector was used at the SPS to investigate the neutral current interactions of high energy neutrinos [14]. Recall that neutral-current neutrino interactions have an outgoing neutrino plus hadrons in the final state. This type of interaction must be distinguished from charged-current neutrino interactions, which have a muon in the final state. Thus, two essential parts of the overall detector are a calorimeter for hadron detection and a muon detector.

The detector consisted of 78 calorimeter subunits surrounded by a frame of magnetized steel and followed by four toroidal iron magnets. Each calorimeter subunit consists of a 3 m $\times$ 3 m $\times$ 8 cm marble plate, a layer of 20 scintillators 15 cm wide and 3 m long, and a layer of 128 proportional drift tubes 3 cm wide and 4 m long. The plate material was

Downloaded from https://www.cambridge.org/core. UNIVERSIDAD AUTONOMA METROPOLITANA, on 15 Nov 2026 at 14:08:38, subject to the Cambridge Core terms of use, available at https://www.cambridge.org/core/terms. https://doi.org/10.1017/9781009290098.015

Downloaded from https://www.cambridge.org/core. UNIVERSIDAD AUTONOMA METROPOLITANA, on 15 Nov 2026 at 14:08:38, subject to the Cambridge Core terms of use, available at https://www.cambridge.org/core/terms. https://doi.org/10.1017/9781009290098.015

Table 14.4. *Examples of fixed target spectrometers*

Spectrometer	Beam	Vertex field	Tracking	Calorimetry	Particle identification	Muon detector	Recoil detector
Neutrino (AGS)	ν	none	PDT	liquid Sc	dE/dx	dipole, PDT	—
CCFR (FNAL)	ν	none	DC	Fe-liquid Sc	—	toroid DC, Sc	—
CDHS (SPS)	ν	none	DC	Fe-Sc	—	1.7 T toroid	—
CHARM (SPS)	ν	none	PDT	marble-PDT streamer tubes, Sc	—	toroid PDT	—
Neutrino (FNAL)	ν	none	PDT flash chambers	PDT flash chambers	—	toroid DC	—
Tagged photon (FNAL)	γ	none	DC, 0.7 T-m, 1.4 T-m dipoles	Pb-Sc, liquid Sc, Fe-Sc	Cer, dE/dx	SC	cyl PC, Sc, liquid Sc

EMC (SPS)	μ	4 T-m	DC, PC 5.2 T-m dipole	Pb-Sc, Fe-Sc	Cer, TOF	—	Streamer chamber, PC, PDT
Multimuon (FNAL)	μ	2 T	DC MWPC	Fe-Sc	—	—	—
E605 (FNAL)	p	none	MWPC, DC dipoles	Pb-Sc, Fe-Sc	RICH	Zn, concrete PDT	—
MPS (FNAL)	p	none	MWPC, DC 1.7 T dipole	Pb-Sc, Fe-Sc	—	1.8 T toroid, MWPC	Pb-glass
LASS (SLAC)	Hadron	2.2 T solenoid	MWPC, Sc 3 T-m dipole	none	Cer, TOF	—	cyl MWPC
MPS II (AGS)	Hadron	4.6 T-m dipole	DC, MWPC Sc	none	Cer, TOF	—	Sc
OMEGA (SPS)	Hadron	1.8 T	MWPC DC, Sc	none	Cer	—	MWPC

Source: Particle Data Group, Major detectors in elementary particle physics, LBL-91, UC-37, 1983.

Downloaded from https://www.cambridge.org/core. UNIVERSIDAD AUTONOMA METROPOLITANA, on 15 Nov 2026 at 14:08:38, subject to the Cambridge Core terms of use, available at https://www.cambridge.org/core/terms. https://doi.org/10.1017/9781009290098.015

Figure 14.7 The European Muon Spectrometer at the SPS. (BH) Beam hodoscope, (V) veto hodoscopes, (P) multiwire proportional chambers, (W) drift chambers, (C) Cerenkov counters, (H1,3,4) scintillator hodoscopes, and H2 calorimeter. (O. Allkofer et al., Nuc. Instr. Meth. 179: 445, 1981.)

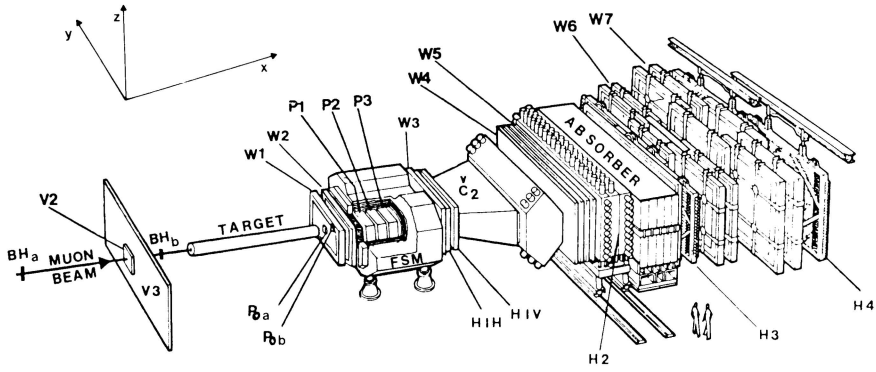
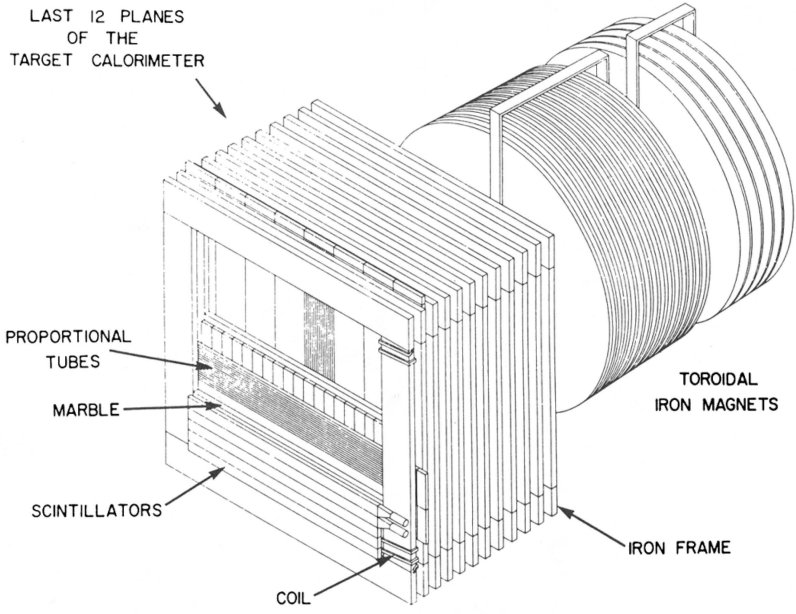


Figure 14.8 The CHARM neutrino detector at the SPS. (A. Diddens et al., Nuc. Instr. Meth. 178: 27, 1980.)



Downloaded from https://www.cambridge.org/core. UNIVERSIDAD AUTONOMA METROPOLITANA, on 15 Nov 2026 at 14:08:38, subject to the Cambridge Core terms of use, available at https://www.cambridge.org/core/terms. https://doi.org/10.1017/9781009290098.015

selected in order to equalize the depth of electromagnetic and hadronic showers. The scintillation counters were required to give a precise measurement of single particle ionization, to sample the shower energy deposition, and to serve as an active target for the neutrino beam. The photomultiplier tube output was split between a discriminator system and ADCs for pulse height measurement. The proportional drift tubes had a cross section of 29×29 mm^2. They could locate muon tracks with an accuracy of 1 mm (rms) and also sampled the shower energy deposition. The readout electronics recorded the charge collected at the sense wire and the drift time for particles traversing the tube.

The iron frames contained a toroidal magnetic field of 15 kG. Forward going muons were momentum analyzed in four toroidal iron discs interspersed with proportional drift tubes. The momentum resolution for 80-GeV/c muons was 25% in the frame magnets and 16% for the forward spectrometer.

All triggers were formed from combinations of scintillation counter signals. The inclusive neutrino trigger required no hits in the first scintillator layer and at least one hit in at least four planes in the rest of the calorimeter. This gave a trigger rate of 0.2 events/10^{13} primary protons on target when using the SPS narrow band neutrino beam.

14.4 Colliding beam spectrometers

In this section we will consider several spectrometers that have been developed for use at colliding beam accelerators. In this case the detectors surround the interaction points of the two beams. Colliding beam spectrometers divide naturally into those used at e^+e^- colliders and at hadron colliders. The major features of some representative e^+e^- detectors are summarized in Table 14.5, while some examples of hadron beam spectrometers are listed in Table 14.6.

We first consider the Mark-J spectrometer at PETRA [15]. The detector was designed to give good measurements of the energy and production angles of electrons, photons, and muons with almost 4π acceptance. A cross-sectional view looking down the beam pipe is shown in Fig. 14.9. The electron and positron beams interact in the area (b). The beam pipe is surrounded by a layer of drift tubes (D), which have a spatial resolution of 300 μm and can determine the longitudinal position of the vertex to ~ 2 mm. Next come three layers of electromagnetic shower counters (S). These contain 18 radiation lengths of interleaved lead and scintillator sheets. The scintillators have PMTs connected to both ends. The relative pulse heights and signal timing from the two PMTs allow an independent

Downloaded from https://www.cambridge.org/core. UNIVERSIDAD AUTONOMA METROPOLITANA, on 15 Nov 2026 at 14:08:38, subject to the Cambridge Core terms of use, available at https://www.cambridge.org/core/terms. https://doi.org/10.1017/9781009290098.015

Downloaded from https://www.cambridge.org/core. UNIVERSIDAD AUTONOMA METROPOLITANA, on 15 Nov 2026 at 14:08:38, subject to the Cambridge Core terms of use, available at https://www.cambridge.org/core/terms. https://doi.org/10.1017/9781009290098.015

Table 14.5. *Examples of e^+e^- colliding beam spectrometers*

Spectrometer	Vertex field	Tracking	Calorimetry	Particle identification	Muon detector	Forward detector
ARGUS (DORIS)	0.8 T solenoid	cyl DC	Pb-Sc	*dE/dx*, TOF	PDT	Pb-Sc
CELLO (PETRA)	1.3 T solenoid	cyl MWPC, cyl DC	Pb-liquid Ar	—	MWPC	Pb-glass Sc, MWPC
CLEO (CESR)	1.0 T solenoid	MWPC, DC	Pb-PDT	TOF, *dE/dx*	DC	Pb-PDT, Sc
Crystal Ball (DORIS)	none	PDT	NaI	—	—	NaI Sc
CUSB (CESR)	none	MWPC	NaI, Pb-glass, MWPC	—	1.5 T toroid Sc, DC	Pb-Sc, NaI
DELCO (PEP)	0.3 T open solenoid	cyl DC, DC	Pb-Sc	Cer, TOF	—	Pb-Sc
HRS (PEP)	1.6 T solenoid	cyl DC, PDT	Pb-Sc, MWPC	Cer, TOF	—	Pb-glass, Pb-Sc, MWPC

JADE (PETRA)	0.5 T solenoid	cyl DC	Pb-glass	*dE/dx*, TOF	DC Sc	Pb-glass, Pb-Sc
MAC (PEP)	0.6 T solenoid	cyl DC	Pb-PWC, Fe-PWC	*dE/dx*, TOF	toroid DC	Fe-PWC, Sc
MARK II (PEP)	0.5 T solenoid	cyl DC	Pb-liquid Ar	TOF	PDT	Pb-PDT, DC, Pb-Sc
MARK III (SPEAR)	0.4 T solenoid	cyl DC	Pb-PWC	*dE/dx*, TOF	PDT	Pb-PWC, Sc
MARK-J (PETRA)	none	PDT, DC	Pb-Sc, Fe-Sc	—	1.7 T toroid DC	DC, Sc
MD-1 (VEPP-4)	1.2 T dipole	MWPC	Fe-MWPC	Cer, TOF	MWPC	NaI, Sc
TASSO (PETRA)	0.5 T solenoid	cyl DC, cyl PWC, DC	Pb-liquid Ar, Pb-Sc	TOF, Cer, *dE/dx*	PDT	Pb-liquid Ar Sc, PDT, Pb-Sc
TPC (PEP)	1.5 T solenoid	cyl DC, TPC	Pb-PWC	*dE/dx*	PDT	PDT, Pb-PWC

Source: Particle Data Group, Major detectors in elementary particle physics, LBL-91, UC-37, 1983.

Downloaded from https://www.cambridge.org/core. UNIVERSIDAD AUTONOMA METROPOLITANA, on 15 Nov 2026 at 14:08:38, subject to the Cambridge Core terms of use, available at https://www.cambridge.org/core/terms. https://doi.org/10.1017/9781009290098.015

Downloaded from https://www.cambridge.org/core. UNIVERSIDAD AUTONOMA METROPOLITANA, on 15 Nov 2026 at 14:08:38, subject to the Cambridge Core terms of use, available at https://www.cambridge.org/core/terms. https://doi.org/10.1017/9781009290098.015

Table 14.6. *Examples of colliding hadron beam spectrometers*

Spectrometer	Vertex field	Tracking	Calorimetry	Particle identification	Muon detector	Forward detector
AFS (ISR)	0.5 T open axial	cyl DC	NaI, U, Cu-Sc	*dE/dx*, Cer	MWPC	Sc
CDF (Tevatron)	1.5 T solenoid	cyl DC	Pb-Sc, Fe-Sc	—	PDT toroid-DC	Pb-PDT, Fe-PDT
SFM (ISR)	1.0 T split field dipole	MWPC	none	*dE/dx*, Cer, TOF	—	MWPC
UA1 (SPS)	0.7 T dipole	cyl DC	Pb-Sc, Fe-Sc	*dE/dx*	PDT	Pb-Sc, DC, Fe-Sc
UA2 (SPS)	none	cyl MWPC, cyl DC, 0.4 T-m toroid + DC	Pb-Sc, Fe-Sc	—	—	Sc

Source: Particle Data Group, Major detectors in elementary particle physics, LBL-91, UC-37, 1983.

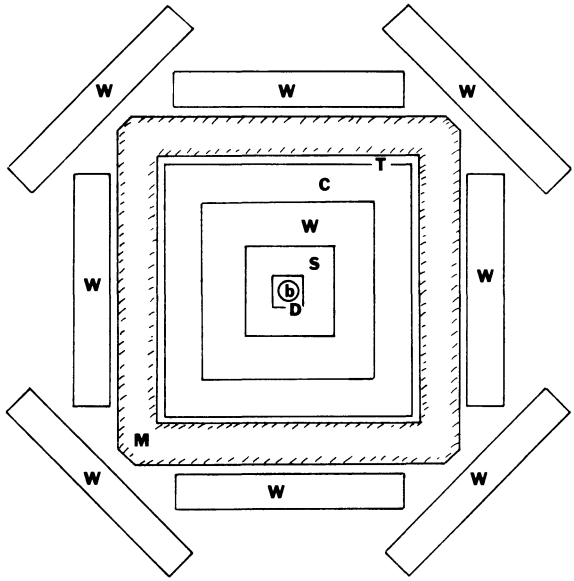
measurement of the longitudinal position of a track. The shower counters signal the presence of an electron or photon.

The electromagnetic calorimeter is followed by a layer of drift chambers (W). These large chambers have 10-cm drift cells arranged in double layers. The layers are grouped in pairs and displaced by half a wire spacing to remove the left–right ambiguity. The chamber gas is argon/isobutane. The chambers have a spatial resolution of 0.6 mm and are used to measure the trajectory of muons through magnetized iron.

Next there is a hadronic calorimeter (C) consisting of iron and scintillator plates, a trigger counter (T), and a magnetized iron toroid (M). The total bending power is 1.7 T-m. The minimum momentum needed to penetrate the iron is 1.3 GeV/c at normal incidence.

Muons produced at small angles along the beam pipe are measured in end cap chambers. The luminosity is measured by detecting small angle e^+e^- elastic scattering (Bhabha) events in lead-glass counter arrays surrounding the beam pipe. The single muon, fast trigger requires signals from the scintillators in the shower counters, a hit in the counter T, and a beam crossing signal. Events that pass the fast trigger must then satisfy a loose track requirement. A microprocessor examines the drift chamber hit information and requires that at least three inner detector double planes have adjacent hits.

Figure 14.9 The MARK-J detector at PETRA. (After D. Barber et al., Phys. Rep. 63: 337, 1980.)



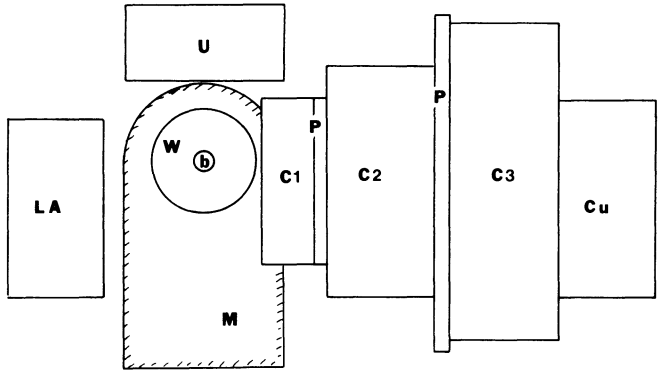
Downloaded from https://www.cambridge.org/core. UNIVERSIDAD AUTONOMA METROPOLITANA, on 15 Nov 2026 at 14:08:38, subject to the Cambridge Core terms of use, available at https://www.cambridge.org/core/terms. https://doi.org/10.1017/9781009290098.015

A second example of a colliding beam spectrometer is the Axial Field Spectrometer (AFS) at the ISR at CERN [16]. The primary objective of this facility was to study phenomena at large transverse momentum. In particular, the experimenters sought to measure the inclusive production of hadrons, electrons, photons, and hadronic jets. Since the ISR circulated beams of hadrons, the interaction rate in the AFS was much higher than that experienced in e^+e^- detectors. Particle fluxes could exceed 10^7 particles per second.

The highest priority in the design of the detector was to provide high resolution electromagnetic and hadronic calorimetry over a wide solid angle. The layout of the detector is shown in Fig. 14.10. As we saw in Section 14.2, the axial field magnet design allows unobstructed access near 90°. The magnetic field integral was 0.5 T-m. Tracking was provided by cylindrical drift chambers near the interaction vertex and MWPCs outside the magnetic field. The spectrometer provided a momentum resolution $\Delta p/p \sim 0.01p$, where p is measured in GeV/c. The azimuthal coordinate was provided by the drift times with a resolution of 200 μm. The coordinate along the wire was given by charge division with a resolution of 1.5 cm.

One arm of the spectrometer was provided with three Cerenkov counters for unambiguous particle identification in the range 2–12 GeV/c. The one nearest the interaction region was a silica-aerogel counter

Figure 14.10 Schematic diagram of the Axial Field Spectrometer at the ISR. Not to scale. (b) Beam pipe, (W) cylindrical drift chambers, (M) axial field magnet, (LA) liquid argon calorimeter, (U) uranium calorimeter, (C1) aerogel Cerenkov counter, (P) MWPC, (C2) high pressure gas Cerenkov counter, (C3) atmospheric gas Cerenkov counter, and (Cu) copper calorimeter. (After H. Gordon et al., Nuc. Instr. Meth. 196: 303, 1982.)



Downloaded from https://www.cambridge.org/core. UNIVERSIDAD AUTONOMA METROPOLITANA, on 15 Nov 2026 at 14:08:38, subject to the Cambridge Core terms of use, available at https://www.cambridge.org/core/terms. https://doi.org/10.1017/9781009290098.015

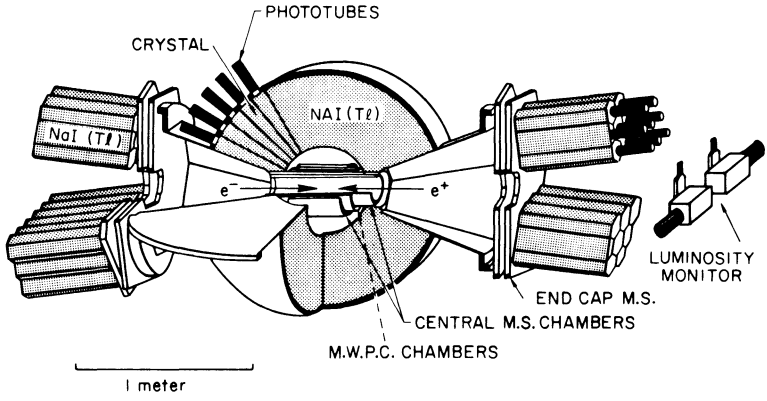
with a refractive index of 1.05. The light from this counter must be wavelength-shifted and transmitted for 2 m to keep the tubes in a low field region. The other two counters used Freon-12 at pressures of 4 and 1 atm.

The calorimeter modules covered 8 sr solid angle around the interaction region. They consisted of an electromagnetic front end followed by a hadronic section. The electromagnetic part consisted of 5 radiation lengths of uranium and scintillator sheets. The scintillator light was wavelength-shifted and transmitted to a PMT at the end of the module. The hadronic part of the calorimeter had 3.6 absorption lengths of uranium, copper, and scintillator sheets. The uranium improved the energy resolution through fission compensation, as discussed in Chapter 11. The energy resolution was $15\%/\sqrt{E}$ for electrons and $34\%/\sqrt{E}$ for pions.

Some specialized detector systems do not use a magnetic field. Figure 14.11 shows a schematic drawing of the Crystal Ball detector, as it was used in experiments at SLAC. The detector has since been moved to an interaction area at PETRA. The detector surrounded one of the e^+e^- interaction regions at the SPEAR colliding beam storage rings [17, 18]. The Crystal Ball was designed to study the spectroscopy of high mass, short-lived particle states by detecting the photons emitted in the transitions between levels. The required large acceptance and high resolution for photon detection was achieved by surrounding the intersection point with a ball of NaI scintillation counters.

The regions closest to the interaction point contained a cylindrical magnetostrictive spark chamber, a cylindrical MWPC for triggering and particle identification, and another cylindrical spark chamber. The crys-

Figure 14.11 The Crystal Ball detector as it was used at SPEAR. (M. Oreglia et al., Phys. Rev. D 25: 2259, 1982.)



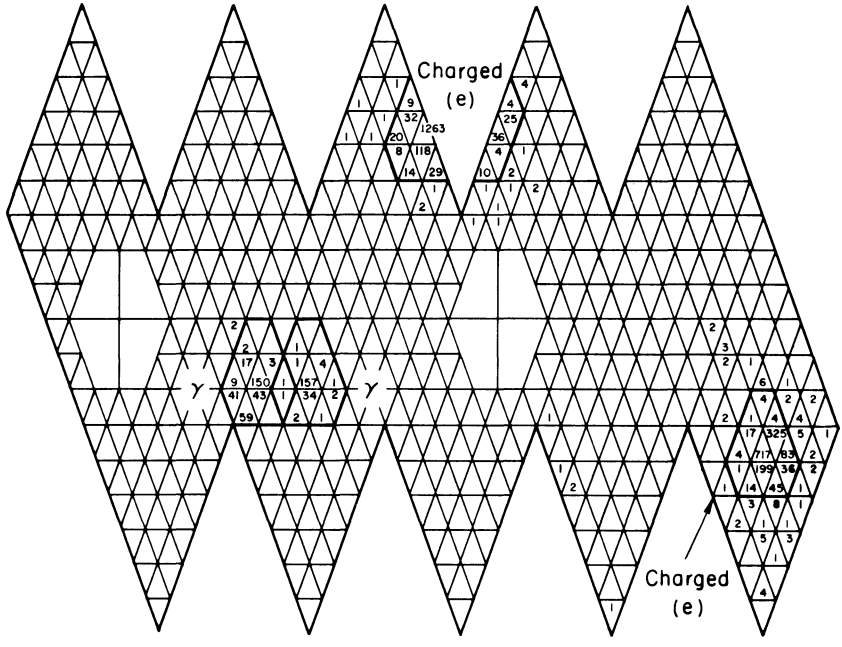
Downloaded from https://www.cambridge.org/core. UNIVERSIDAD AUTONOMA METROPOLITANA, on 15 Nov 2026 at 14:08:38, subject to the Cambridge Core terms of use, available at https://www.cambridge.org/core/terms. https://doi.org/10.1017/9781009290098.015

tal ball itself consisted of 672 NaI (T1) crystals. Each face of a crystal was fitted with white reflecting paper and a sheath of aluminized material for optical isolation. Each crystal was about 16 in. long, corresponding to about 15.7 radiation lengths. The crystals were in the shape of prisms with a small end dimension of 2 in. and a large end dimension of about 5 in. Each counter was connected to a 2-in. photomultiplier tube. The crystals were arranged in the form of a 20-sided regular polyhedron, broken into two separate hemispheres. Some crystals around the beam pipe had to be removed, resulting in 94% of 4π solid angle coverage. End caps, consisting of additional NaI crystals and planar spark chambers, were located approximately 1 m from the interaction point. The end caps increased the NaI solid angle coverage to 98% of 4π. Figure 14.12 shows the pattern of energy deposits in the NaI counters for a $e^+e^-\gamma\gamma$ final state.

The standard deviation on the measurement of the energy of electromagnetic showers was

$$\sigma_E \sim (0.0255 \pm 0.0013)E^{3/4} \qquad \text{GeV}$$

Figure 14.12 Map of the energy deposit in the NaI counters of the Crystal Ball for an $e^+e^-\gamma\gamma$ final state. (M. Oreglia et al., Phys. Rev. D 25: 2259, 1982.)



Downloaded from https://www.cambridge.org/core. UNIVERSIDAD AUTONOMA METROPOLITANA, on 15 Nov 2026 at 14:08:38, subject to the Cambridge Core terms of use, available at https://www.cambridge.org/core/terms. https://doi.org/10.1017/9781009290098.015

This good resolution allowed the experimenters to extract the natural widths of high mass states from the inclusive photon spectrum and to identify certain reactions through constrained kinematic fitting. The direction of a photon could be determined to within 2° of the true polar angle.

The system was triggered using (1) the total energy deposited in the ball, (2) separate energy deposited in two hemispheres, (3) charged particle multiplicity, or (4) back to back energy loss. All triggers were required to come within ±20 ns of the beam crossing signal from SPEAR. The trigger rate was 3–4 Hz at maximum luminosity.

14.5 Nucleon decay spectrometers

A third major class of large detector systems are the nucleon decay spectrometers [19, 20]. These devices differ from those in the previous two sections, since no accelerator beams are involved. Instead a large mass of material is continuously monitored by some type of sensitive detector, either on the surface of the material or interspersed throughout its volume. The detectors generally define a fiducial volume in the center of the monitored material. The signature of a nucleon decay would be an event totally inside the fiducial volume with an energy release of about 940 MeV and with a net momentum of zero.

Table 14.7 summarizes the characteristics of some of the currently operating nucleon decay detectors. The detectors can be separated into three main classes. The first uses water as the source of decaying protons and looks for the Cerenkov light emitted by the charged decay particles in reactions such as $p \rightarrow e^+\pi^0$ or μ^+K^0. The pulse height and arrival time of the PMT signals can be recorded and used to reconstruct the Cerenkov cone. This enables the direction of the particle to be determined. The detector can be triggered by requiring a minimum coincidence of PMT signals.

The second large class of detectors uses a sampling calorimeter made up of some type of gaseous chamber interspersed with plates of material. The monitored material is usually iron plate. Active detectors can be gas proportional chambers or gas detectors operated in a saturated mode. The detectors can be triggered by demanding signals from a minimum number of contiguous planes. The third class of detectors use liquid scintillator. This type of detector has also been used to study solar neutrinos.

The major background in nucleon decay experiments arises from neutrinos and muons produced in the atmosphere by cosmic rays. The muons can be efficiently attenuated by locating the detector far below the surface of the earth. For example, the muon flux at the FREJUS detector

Downloaded from https://www.cambridge.org/core. UNIVERSIDAD AUTONOMA METROPOLITANA, on 15 Nov 2026 at 14:08:38, subject to the Cambridge Core terms of use, available at https://www.cambridge.org/core/terms. https://doi.org/10.1017/9781009290098.015

Downloaded from https://www.cambridge.org/core. UNIVERSIDAD AUTONOMA METROPOLITANA, on 15 Nov 2026 at 14:08:38, subject to the Cambridge Core terms of use, available at https://www.cambridge.org/core/terms. https://doi.org/10.1017/9781009290098.015

Table 14.7. *Examples of nucleon decay detectors*

Detector	Location	Depth (MWe)[a]	Monitored material	Sensitive elements
FREJUS	France	4400	1000 tons iron plates	flashtubes, Geiger tubes
HPW	United States	1500	780 tons water	PMT
IMB	United States	1570	7000 tons water	PMT
Kamiokande	Japan	2700	3000 tons water	PMT
NUSEX	Italy–France	⩾5000	150 tons iron plates	streamer tubes
Kolar	India	7600	140 tons iron plates	gas PC
Baksam	USSR	850	80 tons liquid Sc	PMT
Soudan	United States	1800	30 tons concrete and iron	gas PC
Mt. Blanc	Italy–France	4270	30 tons iron and liquid Sc	PMT, streamer chamber

[a] MWe = Meters of water equivalent.
Source: Particle Data Group, Major detectors in elementary particle physics, LBL-91, UC-37, 1983; S. Weinberg, Sci. Amer., June 1981, p. 64; J. M. Lo Secco, F. Reines, and D. Sinclair, Sci. Amer., June 1985, p. 54.

is 6.2 ± 1.2 muons/day-m^2, a reduction of about 10^6 of the flux at sea level [19]. The outer layer of the detector is used to veto muons coming in from outside the detector. Good nucleon decay events must originate in the fiducial volume of the detector. On the other hand, the neutrino flux is largely unaffected by attenuation in the earth and enters the detector from all directions, regardless of depth. A neutrino interaction inside the fiducial volume may look like a nucleon decay, and this limits the ultimate sensitivity of the experiments.

14.6 Data acquisition

A large detector system is capable of generating immense amounts of digital and analog signals. It is the function of the data acquisition system to control the flow of this information. In general, it is desirable to at least monitor the performance of the experiment as it is happening (online) and to save some of the data for subsequent (offline) analysis. A minimal system for a simple experiment would likely use CAMAC modules as the interface between the experimental equipment and a small computer.

Most experiments make use of a minicomputer to control the online monitoring and data collection for the experiment [21]. Figure 14.13 shows a typical online data acquisition system for a more complicated experiment. The data acquisition system is intimately connected with the trigger. Two constraints may require a highly selective trigger. First, with present technology no more than 10–100 events/sec can be handled and stored on permanent memory. Second, the offline data analysis may require ~ 1 sec/event so that the cost and availability of computer time may restrict the total number of events that can be processed.

The fast trigger detectors include devices such as scintillation counters, Cerenkov counters, and MWPCs. The signals are fed into the trigger logic, where discriminators standardize the pulses, and coincidence units indicate temporal correlations of signals from different detectors. If a good event has occurred, a fast trigger pulse is generated within a few hundred nanoseconds of the event. This causes other triggered devices such as drift chambers, ADCs, and TDCs to be read out.

All of the data is fed into some device that prepares the data in a recognizable fashion and channels it onto a pathway to the computer. Some systems may have a higher level trigger that can make a more complicated decision based on hodoscope matrix correlations or coarse track finding within about 1 μs. Still more complicated decisions may be made using hardware processors or dedicated minicomputers. Some-

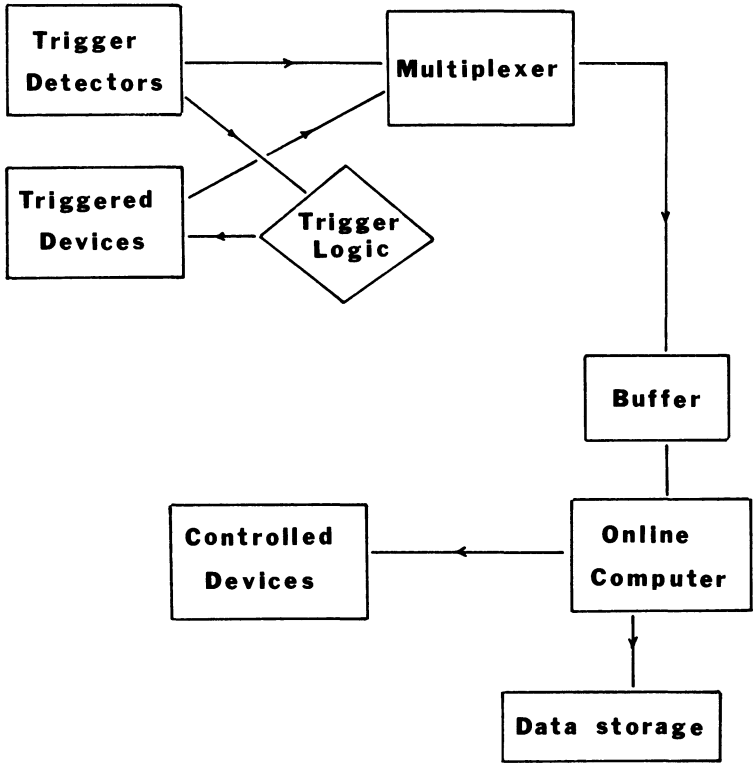
Downloaded from https://www.cambridge.org/core. UNIVERSIDAD AUTONOMA METROPOLITANA, on 15 Nov 2026 at 14:08:38, subject to the Cambridge Core terms of use, available at https://www.cambridge.org/core/terms. https://doi.org/10.1017/9781009290098.015

times these special purpose devices have been designed to emulate the instruction set of a larger, more powerful computer [22]. Then the online filtering program can first be thoroughly tested using the large computer before being used for an experiment. The emulator is slower than the large computer but is much cheaper.

Since the events occur randomly, it may be necessary to provide some temporary storage media or buffer that can store the data from one event while the detector and trigger logic are examining another one. The buffer holds the data until the online computer finishes processing an event and makes the data available for writing onto magnetic tape, at which point it is ready to accept the data from another event. If the trigger rate, computer processing rate, and buffer capabilities are not carefully balanced, many events may occur while the data acquisition system is busy processing a preceding event.

A more sophisticated data acquisition system for a large experiment is outlined in Table 14.8. At the LEP storage ring 25 μs will be available

Figure 14.13 A data acquisition system.



Downloaded from https://www.cambridge.org/core. UNIVERSIDAD AUTONOMA METROPOLITANA, on 15 Nov 2026 at 14:08:38, subject to the Cambridge Core terms of use, available at https://www.cambridge.org/core/terms. https://doi.org/10.1017/9781009290098.015

Table 14.8. *Data acquisition flow*

Level		Characteristic time	Equipment	Data treatment
1	fast trigger	0.1–25 μs	NIM electronics; fast correlation matrices	trigger detector signals, rough topology
2	detector readout	0.025–5 ms	programmable processors using integer arithmetic	drift chambers, analog signals; suppression of empty channels, clusters
3	transfer to computer	5–25 ms	floating point processors, emulator	calculate track vectors, particle reconstruction
4	data recording	0.025–1 sec	minicomputer	filtering based on full event reconstruction

Source: R. Dobinson, Physica Scripta 23: 487, 1981.

Downloaded from https://www.cambridge.org/core. UNIVERSIDAD AUTONOMA METROPOLITANA, on 15 Nov 2026 at 14:08:38, subject to the Cambridge Core terms of use, available at https://www.cambridge.org/core/terms. https://doi.org/10.1017/9781009290098.015

between bunch crossings. Assuming that there is only a small probability for more than one interaction per bunch crossing, trigger decisions that can be made in less than 25 μs will not introduce any deadtime. At each of the higher levels the event selection can be refined. Only the data for events that reach level 4 are recorded [23].

The online computer can perform various auxiliary functions. Analog measuring devices must be calibrated [24]. This generally requires operating the detector in a test beam or under special conditions or injecting a known test signal and measuring the detector's response.

Monitoring of the detectors is a second important auxiliary function of the online computer [24]. The monitoring can be passive, in the sense that the software merely histograms channel hit frequencies and calculates distributions at the same time that the experiment is taking data. Generally this works adequately, so long as sufficient statistics are accumulated for all channels in a reasonable length of time. Otherwise an active monitoring system may be required. An active system injects a test signal as early as possible into the detector elements and then checks that the detectors return the correct response.

Some examples of specific tasks for the monitoring software include checking the high voltages on power supplies, currents in magnets, and scaler contents. This information can be used as part of a feedback loop to adjust the settings of tuneable devices.

References

[1] R. Gluckstern, Uncertainties in track momentum and direction due to multiple scattering and measurement errors, Nuc. Instr. Meth. 24: 381–9, 1963.
[2] K. Amako, K. Kawano, S. Sugimoto, and T. Matsui, High precision field measuring system for a large aperture spectrometer magnet, Nuc. Inst. Meth. 197: 325–30, 1982.
[3] C. Akerlof, R. Hieber, A. Krisch, K. Edwards, L. Ratner, and K. Ruddick, Elastic proton-proton scattering at 90° and structure within the proton, Phys. Rev. 159: 1138–49, 1967.
[4] Some examples of selecting detectors for specific types of e^+e^- physics studies are given in K. Winter, Some detector arrangements at LEP, Physica Scripta 23: 569–78, 1981.
[5] W. Panofsky, The evolution of SLAC and its program, Phys. Today, October, 1983, pp. 34–41.
[6] W. Willis, The large spectrometers, Phys. Today, October 1978, pp. 32–9.
[7] T. Taylor, The choice of spectrometer magnets for LEP, Physica Scripta 23: 459–64, 1981.
[8] D. Anderson, G. Charpak, Ch. Von Gagern, and S. Majewski, Recent developments in BaF_2 scintillator coupled to a low pressure wire chamber, Nuc. Inst. Meth. 225: 8–12, 1984.
[9] Particle Data Group, Major detectors in elementary particle physics, LBL-91, Supplement, UC-37, March 1983.

Downloaded from https://www.cambridge.org/core. UNIVERSIDAD AUTONOMA METROPOLITANA, on 15 Nov 2026 at 14:08:38, subject to the Cambridge Core terms of use, available at https://www.cambridge.org/core/terms. https://doi.org/10.1017/9781009290098.015

[10] P. Darriulat, Large transverse momentum hadronic processes, Ann. Rev. Nuc. Part. Sci. 30: 159–210, 1980.
[11] C. Fabjan and T. Ludlam, Calorimetry in high energy physics, Ann. Rev. Nuc. Part. Sci. 32: 335–89, 1982.
[12] S.L. Wu, e^+e^- Physics at PETRA — The first five years, Phys. Rep. 107: 59–324, 1984.
[13] O.C. Allkofer, J.J. Aubert, G. Bassompierre, K.H. Becks, Y. Bertsch, C. Besson, C. Best, E. Bohm, D.R. Botterill, F.W. Brasse, C. Broll, J. Carr, B. Charles, R.W. Clifft, J.H. Cobb, G. Coignet, F. Combley, J.M. Crespo, P.F. Dalpiaz, P. Dalpiaz, W.D. Dau, J.K. Davies, Y. Declais, R.W. Dobinson, J. Drees, A. Edwards, M. Edwards, J. Favier, M.I. Ferrero, J.H. Field, W. Flauger, E. Gabathuler, R. Gamet, J. Gayler, P. Ghez, C. Gossling, J. Hass, U. Hahn, K. Hamacher, P. Hayman, M. Henckes, H. Jokisch, J. Kadyk, V. Korbel, M. Maire, L. Massonnet, A. Melissinos, W. Mohr, H.E. Montgomery, K. Moser, R.P. Mount, M. Moynot, P.R. Norton, A.M. Osborne, P. Payre, C. Peroni, H. Pessard, U. Pietrzyk, K. Rith, M.D. Rousseau, E. Schlosser, M. Schneegans, T. Sloan, M. Sproston, W. Stockhausen, H.E. Stier, J.M. Thenard, J.C. Thompson, L. Urban, M. Vivargent, G. von Holtey, H. Wahlen, E. Watson, V.A. White, D. Williams, W.S.C. Williams, and S.J. Wimpenny, A large magnetic spectrometer system for high energy muons, Nuc. Inst. Meth. 179: 445–66, 1981.
[14] A.N. Diddens, M. Jonker, J. Panman, F. Udo, J.V. Allaby, U. Amaldi, G. Barbiellini, A. Baroncelli, V. Blobel, G. Cocconi, W. Flegel, W. Kozanecki, E. Longo, K.H. Mess, M. Metcalf, J. Meyer, R.S. Orr, F. Schneider, A.M. Wetherell, K. Winter, F.W. Busser, P.D. Gall, H. Grote, P. Heine, B. Kroger, F. Niebergall, K.H. Ranitzsch, P. Stahelin, V. Gemanov, E. Grigoriev, V. Kaftanov, V. Khovansky, A. Rosanov, R. Biancastelliok, B. Borgia, C. Bosio, A. Capone, F. Ferroni, P. Monacelli, F. DeNotaristefani, P. Pistilli, C. Santoni, and V. Valente, A detector for neutral current interactions of high energy neutrinos, Nuc. Instr. Meth. 178: 27–48, 1980.
[15] D.P. Barber, U. Becker, H. Benda, A. Bohm, J.G. Branson, J. Bron, D. Buikman, J.D. Burger, C.C. Chang, H.S. Chen, M. Chen, C.P. Cheng, Y.S. Chu, R. Clare, P. Duinker, G.Y. Fang, H. Fesefeldt, D. Fong, M. Fukushima, J.C. Guo, A. Hariri, G. Herten, M.C. Ho, H.K. Hsu, R.W. Kadel, W. Krenz, J. Li, Q.Z. Li, M. Lu, D. Luckey, C.M. Ma, D.A. Ma, G.G.G. Massaro, T. Matsuda, H. Newman, M. Pohl, F.P. Poschmann, J.P. Revol, M. Rohde, H. Rykaczewski, K. Sinram, H.W. Tang, L.G. Tang, Samuel C.C. Ting, K.L. Tung, F. Vannucci, X.R. Wang, P.S. Wei, M. White, G.H. Wu, T.W. Wu, J.P. Xi, P.C. Yang, C.C. Yu, X.H. Yu, N.L. Zhang, and R.Y. Zhu, Physics with high energy electron-position colliding beams with the Mark J. detector, Phys. Rep. 63: 337–91, 1980.
[16] H. Gordon, R. Hogue, T. Killian, T. Ludlam, M. Winik, C. Woody, D. Burckhart, V. Burkert, O. Botner, D. Cockerill, W.M. Evans, C.W. Fabjan, T. Ferbel, P. Frandsen, A. Hallgren, B. Heck, M. Harris, J.H. Hilke, H. Hofmann, P. Jeffreys, G. Kantardjian, G. Kesseler, J. Lindsay, H.J. Lubatti, W. Molzon, B.S. Nielsen, P. Queru, L. Rosselet, E. Rosso, A. Rudge, R.H. Schindler, T. Taylor, J. v.d. Lans, D.W. Wang, Ch. Wang, W.J. Willis, W. Witzeling, H. Boggild, E. Dahl-Jensen, I. Dahl-Jensen, Ph. Dam, G. Damgaard, K.H. Hansen, J. Hooper, R. Moller, S.O. Nielsen, L.H. Olsen, B. Schistad, T. Akesson, S. Almehed, G. von Dardel, G. Jarlskog, B. Lorstad, A. Melin, U. Mjornmark, A. Nilsson, M.G. Albrow, N.A. McCubbin, M.D. Gibson, J. Hiddleston, O. Benary, S. Dagan, D. Lissauer, and Y. Oren, The Axial Field Spectrometer at the CERN ISR, Nuc. Instr. Meth. 196: 303–13, 1982.
[17] E. Bloom and C. Peck, Physics with the Crystal Ball detector, Ann. Rev. Nuc. Part. Sci. 33: 143–97, 1983.

Downloaded from https://www.cambridge.org/core. UNIVERSIDAD AUTONOMA METROPOLITANA, on 15 Nov 2026 at 14:08:38, subject to the Cambridge Core terms of use, available at https://www.cambridge.org/core/terms. https://doi.org/10.1017/9781009290098.015

[18] M. Oreglia, E. Bloom, F. Bulos, R. Chestnut, J. Gaiser, G. Godfrey, C. Kiesling, W. Lockman, D.L. Scharre, R. Partridge, C. Peck, F.C. Porter, D. Antreasyan, Yi-Fan Gu, W. Kollmann, M. Richardson, K. Strauch, K. Wacker, D. Aschmann, T. Burnett, C. Newman, M. Cavalli-Sforza, D. Coyne, H. Sadrozinski, R. Hofstadter, I. Kirkbride, H. Kolanoski, K. Konigsmann, A. Liberman, J. O'Reilly, B. Pollock, and J. Tompkins, Study of the reaction $\Psi' \to \gamma\gamma J/\Psi$, Phys. Rev. D 25: 2259–77, 1982.
[19] M. Nieto, W. Haxton, C. Hoffman, E. Kolb, V. Sandberg, and J. Toevs (eds.), *Science Underground,* AIP Conf. Proc. No. 96, New York: AIP, 1983.
[20] D.H. Perkins, Proton decay experiments, Ann. Rev. Nuc. Part. Sci. 34: 1–52, 1984.
[21] F. Kirsten, Computer interfacing for high energy physics experiments, Ann. Rev. Nuc. Sci. 25: 509–54, 1975.
[22] P. Kunz, Use of emulating processors in high energy physics, Physica Scripta 23: 492–98, 1981.
[23] Many of the things that were considered in the design of the data acquisition system for the European Muon Spectrometer are described in R. Dobinson, Practical Data Acquisition Problems in Large High Energy Physics Experiments, Proc. 1980, CERN School of Computing, CERN Report 81-03, 1981, pp. 325–61.
[24] M. Breidenbach, Calibration, monitoring, and control of complex detector systems, Physica Scripta 23: 508–11, 1981.

Exercises

1. Tracking is to be done with a set of 10 chambers equally spaced over 5 m in a 1-T magnetic field. What is the resolution on the measurement of a 20-GeV/c particle if the chambers have 200 μm spatial resolution? Estimate the contribution of multiple scattering to the momentum resolution if each of the chambers contains 0.05 radiation lengths of material.

2. Consider a rectangular dipole as shown in Fig. 14.2. Prove Eq. 14.11. Calculate the displacement Δx in the direction along the face of the magnet between the particle's entry and exit points.

3. Estimate the deflection angle of a 50-GeV muon that passes radially through a 2-m-wide toroidal field. Assume the toroid has a field of 0.5 T at the inner toroid radius of 1 m.

4. Design a fixed target spectrometer to measure inclusive hadron production from a hadron beam. Specify the locations and characteristics of any counters, tracking chambers, magnets, particle identification detectors, or calorimeters that are used. What trigger would you use?

5. Design a colliding beam spectrometer that can be used to search for the existence of the hypothetical Higgs particle H using the reaction

Downloaded from https://www.cambridge.org/core. UNIVERSIDAD AUTONOMA METROPOLITANA, on 15 Nov 2026 at 14:08:38, subject to the Cambridge Core terms of use, available at https://www.cambridge.org/core/terms. https://doi.org/10.1017/9781009290098.015

$$e^+e^- \rightarrow \mu^+\mu^- H^0$$

6. An experiment is to be done at a colliding beam accelerator with bunched beams and a luminosity per bunch collision L (i.e., L is the instantaneous luminosity $\mathscr{L}$ integrated over the bunch collision time). Suppose that it is not possible to interpret events unambiguously if more than one interaction occurs per bunch collision.
   a. If the cross section for interesting processes is σ and the total cross section is σ_t, then find the mean number of interesting events per bunch collision.
   b. What is the probability of getting one and only one interesting event per bunch collision?
   c. What is the mean number of background events per bunch collision?
   d. What is the probability of getting zero background events per bunch collision?
   e. What is probability of getting one and only one interesting event per bunch collision and nothing else?

Downloaded from https://www.cambridge.org/core. UNIVERSIDAD AUTONOMA METROPOLITANA, on 15 Nov 2026 at 14:08:38, subject to the Cambridge Core terms of use, available at https://www.cambridge.org/core/terms. https://doi.org/10.1017/9781009290098.015